European Journal of Mechanics / B Fluids 78 (2019) 194–202

Contents lists available at ScienceDirect

European Journal of Mechanics / B Fluids

journal homepage: www.elsevier.com/locate/ejmflu

Dielectrophoretic interaction of circular particles in a uniform electric field

N. Tofighi [a,b,*], M. Ozbulut [a,c], A. Suleman [b], J.J. Feng [d,e], M. Yildiz [a,f,g,**]

[a] Faculty of Engineering and Natural Sciences (FENS), Sabanci University, Tuzla, 34956, Istanbul, Turkey
[b] Department of Mechanical Engineering, University of Victoria, Victoria, BC V8W 2Y2, Canada
[c] Faculty of Engineering, Piri Reis University, Postane, Tuzla, 34940, Istanbul, Turkey
[d] Department of Mathematics, University of British Columbia, Vancouver, BC V6T 1Z2, Canada
[e] Department of Chemical and Biological Engineering, University of British Columbia, Vancouver, BC V6T 1Z3, Canada
[f] Integrated Manufacturing Technologies Research and Application Center, Sabanci University, Tuzla 34956, Istanbul, Turkey
[g] Composite Technologies Center of Excellence, Sabanci University-Kordsa, Istanbul Technology Development Zone, Pendik, 34906, Istanbul, Turkey

HIGHLIGHTS

- Dielectrophoretic chaining trajectory of a dispersed phase is studied.
- Interaction forces of two particles in quiescent fluid are investigated in detail.
- Effects of Reynolds number and particle properties are studied.

GRAPHICAL ABSTRACT

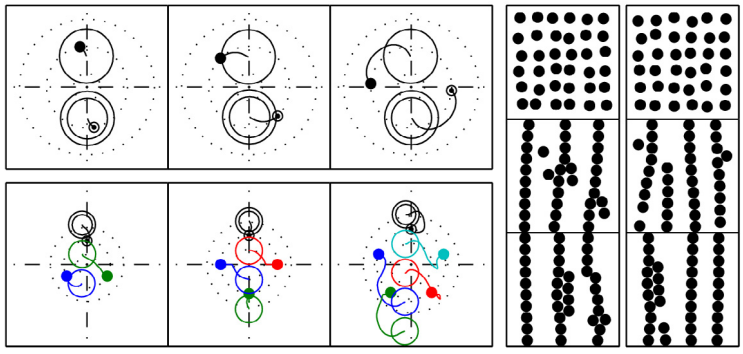

ARTICLE INFO

Article history:
Received 12 January 2018
Received in revised form 14 June 2019
Accepted 6 July 2019
Available online 15 July 2019

Keywords:
Electrohydrodynamics
Smoothed particle hydrodynamics
Fluid–particle interaction
Particle chaining
Dielectrophoresis

ABSTRACT

A two-dimensional incompressible smoothed particle hydrodynamics scheme is used to simulate the interaction of micron-sized particles suspended in quiescent medium. A uniform electric field is applied to the particles, causing them to approach one another due to dielectrophoretic forces and form a chain. Both fluid and particles are assumed to be polarizable and non-conductive where the permittivity of the fluid is assumed to be lower than that of the particles. The numerical scheme is validated by comparing its predictions for simpler case of a pair of particles with results available in the literature. The effects of initial orientation, Reynolds number and differences in particle permittivity on the chaining behavior are studied afterwards. The results show that the particles may follow a convergent or divergent–convergent trajectory, depending on the initial orientation of the particle pair with the electric field. Increasing the field intensity in low-Reynolds regime expedites the chaining process without affecting the particle trajectory. However, the particles may diverge at larger Reynolds numbers. Assigning different permittivities to particles skews the chaining position toward the particle with lower permittivity. Simulating the process for multiple particles results in longer chains branching and encompassing the entire computational domain, much like those observed in experiments.

1. Introduction

Exposing a particle suspended in quiescent background fluid to a sufficiently large and locally non-uniform electric field results in spontaneous motion of the particle. This process, known as dielectrophoresis (DEP), was initially observed in electrorheological

* Corresponding author at: Department of Mechanical Engineering, University of Victoria, Victoria, BC V8W 2Y2, Canada.
** Corresponding author at: Faculty of Engineering and Natural Sciences (FENS), Sabanci University, Tuzla, 34956, Istanbul, Turkey.
E-mail addresses: nima@sabanciuniv.edu (N. Tofighi), mozbulut@pirireis.edu.tr (M. Ozbulut), suleman@uvic.ca (A. Suleman), james.feng@ubc.ca (J.J. Feng), meyildiz@sabanciuniv.edu (M. Yildiz).

https://doi.org/10.1016/j.euromechflu.2019.07.002
0997-7546/

fluids where an electric field is employed to control fluid viscosity [1]. DEP is of great importance in manipulation and assembly of colloidal particles and biological cells [2]. Due to better control and faster response when compared to other means, DEP has become one of the more popular methods for characterization and actuation of particles [3].

Filtering, trapping, sorting and focusing of suspended particles and biological cells within a fluid flow comprise a few applications of DEP particle manipulation [4,5]. Another application of DEP is in the assembly of particles into different microstructures [2]. Hermanson et al. [6] and Xiong et al. [7] assembled colloidal particles into functional microwires. Lumsdon et al. [8] have generated two-dimensional crystals using silica and latex particles between coplanar electrodes. Yang et al. [9] created cardiac tissue-like structures by alignment and aggregation of cardiac myocytes inside a microfluidic chip. Markx et al. [10] used DEP to create cell aggregates with a defined internal architecture similar to that of a putative hematon and showed that the cells remain viable and active after the assembly. Formation of biocomposites from live cells and functionalized particles is another example of DEP application [11,12]. Pethig [3] and Velev et al. [2] provide a comprehensive review of DEP applications.

A pair of neutrally buoyant particles suspended in quiescent medium subject to an external electric field is one of the basic configurations used for the study of DEP assembly. The proximity of the particles distorts the local electric field, causing a force imbalance which in turn results in relative motion of the particles and their eventual chaining [13]. Because it is difficult to isolate and track individual particles, very few experiments have been done on this basic configuration. Hwang et al. [14] experimentally observe the trajectories of particles for several initial configurations. In other experiments, Mittal et al. [15] measure the interparticle forces of aligned particles during their approach. Some analytical works also deal with the interaction of particle pairs. Parthasarathy and Klingenberg [1] provide an analytical solution of the DEP forces between interacting particles in an electrorheological setup. Kang and Li [16] give a similar relation to that of Parthasarathy and Klingenberg [1] for DEP forces. Additionally, they derive the trajectories of particles. However, due to complexity of the particle interactions, these analytical solutions require empirical coefficients and are limited to larger separations between particles.

When compared to the experimental and analytical methods, numerical simulations provide considerable flexibility in the study of DEP interaction of a particle pair. Recent numerical studies use Maxwell stress tensor to account for electrical forces and assume thin electric double layers. The chaining behaviors of conductive and non-conductive particles are simulated for both alternating current (AC) and direct current (DC) electric fields. Ai and Qian [17] consider the behavior of a pair of non-polarizable identical circular particles and observe their chaining trajectory and velocities. Xie et al. [18] conduct similar simulations assuming finite permittivity for the particles. Keeping the electrical properties identical, they study the interaction of up to three particles with different diameters. Kang [19] examines the interaction of particles having zero permittivity and various conductivity values and reports their trajectory and local snapshots of electrical forces on the particle surfaces. In a similar work by Hossan et al. [20], the chaining behavior of up to three polarizable particles with either similar or different conductivities is investigated. In addition to circular particles, House et al. [21] examine the chaining trajectory and orientation of a pair of elliptic particles. The aforementioned works were all carried out in DC electric fields. Similar studies in DEP chaining of particles in AC fields are carried out by Ai et al. [22] and Hossan et al. [23].

Despite the large number of numerical studies in DEP chaining of particle pairs, the discussion on DEP forces during the course of chaining and their relation to orientation with the electric field is inconclusive and limited to analytical works of [1,16]. Additionally, most of the above studies neglect the convective terms in fluid motion. As such, higher Reynolds flows encountered in electrorheological systems remain largely unstudied. Furthermore, interactions between particles of different permittivities have not been examined thoroughly, although such binary mixtures of particles are important to potential applications [11,12]. In this study, we aim to improve on these aspects of the numerical studies on the DEP chaining of particle pairs using Smoothed Particle Hydrodynamics method (SPH) [24]. In addition, we briefly investigate the interactions between larger numbers of particles. The parameters of the studies conducted here are chosen such that the results are valid for micro-scale particles [17,18]. Further motivations for the current study are provided at the beginning of each section analyzing the results.

In this work we use a two-dimensional isothermal incompressible SPH (ISPH) scheme based on the projection method and corrected derivatives [25–27]. The coupling of the fluid and solid phases is carried out through the viscous penalty method in conjunction with rigidity constraints [28]. Both fluid and particles are assumed to be dielectric materials subject to an external DC electric field [29]. The particles have larger permittivity than the surrounding fluid in most cases considered here. Particles having lower permittivity than the fluid behave qualitatively the same way and thus will not be discussed separately, except when validating our simulation results. Sections 2 and 3 provide the mathematical formulation used in this study. Simulation results are presented in Section 4 and concluding remarks are drawn in Section 5. From this point forward, the term "particle" will refer to the SPH particles used to discretize the computational domain while the solid objects will be referred to as discs.

2. Geometry and characteristic scales

The simplest form of DEP interaction is between two closely positioned neutrally buoyant circular discs. Fig. 1 provides a schematic of the problem where subscripts $\square_1$ and $\square_2$ are used to denote discs 1 and 2, respectively. The origin of coordinate axes (x, y) is placed at the center of computational domain. An additional Cartesian coordinate system is attached to disc 1 which points in parallel (n) and normal (s) directions to the line connecting the disc centers. The discs with radii of r_1 and r_2 are suspended in a square cavity of side length $H = 20r_1$. The distance between disc centers is referred to as L_c and the surface-to-surface distance is defined as $L_s = L_c - r_1 - r_2$. A constant electric potential difference of $\Delta\phi$ is applied between the horizontal walls, shown as continuous lines, resulting in an undisturbed electric field in the vertical direction. Initially, the discs are placed at a distance $L_s/2 = r_1/2$ from the center of computational domain and their center-to-center line has an initial angle of θ with the electric field. Side walls, shown in dashed lines, are insulated and electric field lines are parallel to these walls. All bounding walls are subject to no-slip and no penetration conditions.

Following Saville [30], we define a characteristic velocity u_c by balancing viscous $(\mu_c u_c / l_c^2)$ and electric $(\varepsilon_c E_c^2 / l_c)$ forces as

$$u_c = \frac{\varepsilon_c l_c E_c^2}{\mu_c}. \tag{1}$$

All other characteristic values are chosen as

$$\rho_c = \rho_0, \quad \mu_c = \mu_0, \quad \varepsilon_c = \varepsilon_0, \quad l_c = r_1,$$
$$t_c = l_c/u_c, \quad E_c = E_\infty = \Delta\phi/H, \quad p_c = \rho_c u_c^2, \tag{2}$$

where ρ is density, μ is viscosity, ε is electrical permittivity, l is length, t is time, E is electric field intensity and p is pressure.

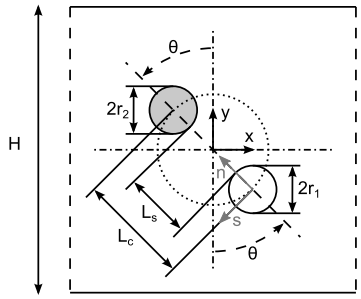

Fig. 1. Schematic of the DEP chaining of two circular discs. Discs 1 and 2 are colored in white and gray, respectively. The (n, s) coordinate axes attached to disc 1 are shown in gray.

Subscripts $\square_c$ and $\square_0$ denote characteristic and fluid phase values, respectively. We will only consider neutrally buoyant discs in this study.

The dimensionless values governing the test case are

$$\mathcal{R} = \frac{r_1}{H}, \quad \mathcal{R}_r = \frac{r_2}{r_1},$$
$$\mathcal{P} = \frac{\varepsilon_1}{\varepsilon_0}, \quad \mathcal{P}_r = \frac{\varepsilon_2}{\varepsilon_1}, \tag{3}$$

along with the Reynolds number,

$$\mathrm{Re} = \rho_0 \varepsilon_0 \left(\frac{r_1 E_\infty}{\mu_0}\right)^2. \tag{4}$$

In addition to Re, balancing electrical $(\varepsilon_c E_c^2/l_c)$ and inertial $(\rho_c u_c^2/l_c)$ terms results in electro-inertial number $\mathrm{Ei}_c = \varepsilon_c E_c^2/\rho_c u_c^2$ [31]. With the velocity scale of Eq. (1), however, it is identical to the inverse of Re.

Through this study we assume the discs have identical radii hence $\mathcal{R}_r = 1$. Domain size and boundary conditions remain unchanged for cases with more than two discs of Section 4.4. The arrangement of discs and dimensionless values will be discussed in the relevant sections.

3. Mathematical method

Equations governing an incompressible and isothermal flow subject to an external electric field may be written in dimensionless form as

$$\nabla \cdot \mathbf{u} = 0, \tag{5}$$

$$\frac{\mathrm{D}\mathbf{u}}{\mathrm{D}t} = -\nabla p + \frac{1}{\mathrm{Re}}\left[\nabla \cdot \boldsymbol{\tau} + \mathbf{f}_{(e)}\right], \tag{6}$$

where vectors and tensors are shown in bold and $\mathrm{D}/\mathrm{D}t = \partial/\partial t + \mathbf{u}\cdot\nabla$ represents the material time derivative. Here, $\boldsymbol{\tau}$ is the viscous stress tensor,

$$\boldsymbol{\tau} = \mu\left[\nabla\mathbf{u} + (\nabla\mathbf{u})^\dagger\right], \tag{7}$$

where superscript $\square^\dagger$ denotes the transpose operation while $\mathbf{f}_{(e)}$ is the electric force vector calculated through divergence of Maxwell stress tensor [30].

Assuming small dynamic currents and neglecting magnetic induction effects, the electric field is irrotational and may be represented by the gradient of an electric potential, $\mathbf{E} = -\nabla\phi$. A further assumption of slow electric relaxation compared to viscous relaxation allows for the electric potential to be computed through

$$\nabla \cdot (\varepsilon \nabla \phi) = 0, \tag{8}$$

resulting in the following form of the electric force [32],

$$\mathbf{f}_{(e)} = -\frac{1}{2}\mathbf{E}\cdot\mathbf{E}\nabla\varepsilon. \tag{9}$$

To distinguish between different phases, a color function $\hat{c}^\alpha$ is defined for each of the solid and fluid bodies such that it is unity for the region containing phase α and zero for all other regions. As mentioned before, $\alpha = 0$ denotes the fluid phase while $\alpha \geq 1$ refer to the discs. Thermodynamic variables and transport coefficients are interpolated using the corresponding color function values [27].

The fluid and solid bodies are treated as liquids of different viscosity according to the viscous penalty method [33] where a viscosity ratio of one hundred is used [28]. Rigidity constraints derived from conservation of momenta are applied to individual solid regions to ensure a rigid behavior [28,34]. To maintain enough particles for resolving the flow and electric fields in the fluid, the minimum distance between solid surfaces (walls or discs) is limited to two particle spacings using a local repulsive force [28]. Details of the numerical solution procedure is provided in [28,35].

4. Results

To assess the ability of the proposed method in capturing the chaining behavior of rigid discs, the results of current simulations are compared to those provided in [17,18]. Identical discs are released from an initial angle of $\theta_i = 85°$ with Reynolds number set to 0.007. Two permittivity ratios, $\mathcal{P} = 1/40$ and 40 are selected for comparison. The fluid is discretized with particles arranged on a uniformly spaced Cartesian grid with a particle spacing of δ_p. Rigid bodies are discretized with particles conforming to disc boundaries, positioned along concentric circles at uniform radial spacing δ_p around the disc center. The number of particles on each circle is varied to keep the separation distance between the particles close to δ_p along each of the circles [28]. Here, the smoothing length is taken as $h = 1.6\delta_p$ [26].

When a disc more polarizable than the surrounding fluid is placed in a non-uniform electric field, it moves toward regions of higher field gradient. This phenomenon is known as positive DEP. The reverse, called negative DEP, is true for discs less polarizable than the surrounding fluid [2]. Two discs placed closely in a uniform electric field affect the surrounding field and create gradients that move the discs. If both discs are either more polarizable or less polarizable than the surrounding fluid, the DEP forces will align them with the electric field. Fig. 2 plots the trajectory of disc 1 while the pair is aligning with the electric field for different particle spacings against simulation results in [17,18]. A filled circle marker shows the initial position of the disc. It is seen that reducing particle spacing to $\delta_p \leq 0.1$ and $\delta_p \leq 0.13$ for $\mathcal{P} = 1/40$ and $\mathcal{P} = 40$, respectively, results in very small difference in the trajectory of the discs. As such, $\delta_p = 0.1$ and $\delta_p = 0.13$ are considered adequate for $\mathcal{P} = 1/40$ and $\mathcal{P} = 40$, respectively. The reason for higher resolution required for $\mathcal{P} = 1/40$ lies in the way the weighted harmonic mean interpolation skews the transition region toward larger permittivity values. For $\mathcal{P} = 1/40$, the transition region shifts toward the fluid particles and a finer resolution is needed to keep the transition close to the disc boundary. The trajectory of the discs at the converged particle spacings are in agreement with those of [17,18]. Xie et al. [18] report their results for both 1/40 and 40 ratios while Ai and Qian [17] limit their study to non-polarizable particles. Xie et al. [18] compare their results for $\mathcal{P} = 1/40$ and $\mathcal{P} = 0$ and report negligible difference, showing that discs at $\mathcal{P} = 1/40$ are essentially non-polarizable.

Hereafter, we only consider discs that have larger permittivities than the surrounding fluid and a reference permittivity ratio

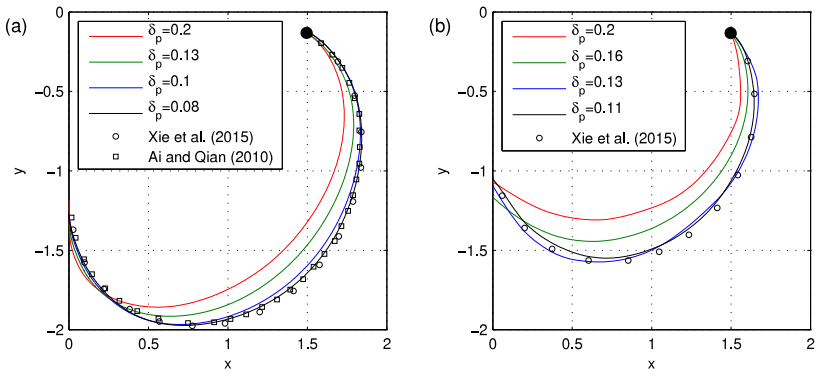

Fig. 2. Validation of particle resolution and comparison of simulation results with disc 1 trajectory data given by Xie et al. [18] and Ai and Qian [17] for $\mathcal{P} = 1/40$ (a) and $\mathcal{P} = 40$ (b). The starting position and trajectory of disc 2 is symmetric with respect to the center of computational domain at (0, 0).

Table 1
Elapsed time for reaching θ_f for different starting orientations.

θ_i	10°	30°	45°	60°	85°
t_f	8.13	8.62	10.94	12.22	37.08

of $\mathcal{P} = 40$ is chosen. The numerical results consist of four studies. First, the effect of initial orientation of center-to-center line with the electric field is inspected. Then the effect of Reynolds number on the behavior of the discs will be examined. Reynolds numbers up to 116.1 are simulated to provide a better understanding of the chaining behavior. The third case investigates the effects of dissimilarities in electrical properties. Finally, the interactions between more than two discs are investigated.

4.1. The effect of initial orientation

To our knowledge, the most detailed study on the effect of initial orientation on the trajectory of chaining discs is carried out by Kang [19]. However, he only shows the surface distribution of the DEP forces on the discs at $\theta = 45°$ and $L_c = 4$ snapshots and no time variation is examined. Ai et al. [17,22] examine the time variation of DEP force, however, they only consider the forces in the direction of electric field and for $\theta_i = 0°$ and 45°. On the other hand, the analytical solutions of [1,16] require prior knowledge of the electric field distribution or empirical relations. In this section, the behavior of the discs at five starting angles of 10°, 30°, 45°, 60° and 85° with the electric field is examined. The two discs are identical with $\mathcal{P} = 40$, and the Reynolds number is fixed at Re = 0.007. Simulation results are shown until the center-to-center line connecting the discs reaches $\theta = 1°$, at which point we consider the discs to be chained. The elapsed time until $\theta_f = 1°$ is referred to as the chaining time t_f. Table 1 provides the chaining times for each starting orientation. Increasing the initial angle results in larger chaining time with a significant increase from $\theta_i = 60°$ to 85°.

Fig. 3 provides the trajectories of the discs with respect to θ. As expected, the identical discs rotate and align with the electric field axisymmetrically. With the exception of $\theta_i = 85°$, the distance between the discs decreases during their travel. For $\theta_i = 85°$, the distance between the discs increases initially, reaching a maximum of $L_c = 3.65$ at $\theta = 53°$ before dropping to $L_c = 2.25$ at θ_f. Such behavior has been reported in numerical simulations of conductive disc pairs [19,20] as well as non-conductive disc pairs [17,18]. This also explains the much longer chaining time when starting from an initial angle of 85°, as observed in Table 1.

A better understanding of the effect of initial orientation on the behavior of the discs may be obtained by observing the changes in electrical forces with respect to θ and L_c. Fig. 4 plots the DEP force component per unit volume in the center-to-center direction $f_{(en)}$, where a positive value indicates an attractive force, as well as the electric force component normal to the center-to-center direction $f_{(es)}$, which results in a clockwise rotation if its value is positive. Directions for (n, s) coordinate axes are provided in Fig. 1. Since the forces are identical in magnitude for both discs, only the DEP forces on disc 1 are shown. It is expected that as the discs align with the electric field, the center-to-center force reaches a maximum while the component causing the rotation vanishes [1,16].

Fig. 4-a shows that the center-to-center component of DEP force remains attractive throughout the trajectory for cases with $\theta_i \leq 45°$. Cases starting at 60° and 85° experience an initially repulsive $f_{(en)}$. The angular span of the repulsive force is rather short for $\theta_i = 60°$ and is not enough to cause a substantial increase in the initial separation between the discs. For $\theta_i = 85°$, on the other hand, approximately one third of the traversed angle is spent in the repulsive region and this results in a significant increase in separation as shown in Fig. 3-b. It is worth noting that for both $\theta_i = 60°$ and 85° the repulsive force changes to an attractive one at about $\theta = 53°$, which also corresponds to the angle when the trajectory of the case $\theta_i = 85°$ changes from a diverging path to a converging one (Fig. 3-b). The analytical solution of [1,16] suggests that $f_{(en)}$ changes direction according to the sign of $3\cos^2\theta - 1$, which corresponds to $\theta \approx 54.7°$. Hwang et al. [14] suggest an angle between $\theta = 52.6°$ and 53.4° based on their experimental observations. Both values are fairly close to the current numerical result of $\theta \approx 53°$. The maximum value of $f_{(en)}$ is comparable for all cases, regardless of the starting orientation and resides in the final portions of the travel.

The rotational component of DEP force $f_{(es)}$ versus θ is plotted in Fig. 4-b. Unlike $f_{(en)}$, the largest magnitude of $f_{(es)}$ is dependent on the starting orientation of the discs. According to the analytical solution, $f_{(es)}$ changes with $\sin 2\theta/L_c^4$ and reaches a maximum when $\theta = 45°$ [1,16]. Our results for $\theta_i \leq 45°$ exhibit the largest rotational DEP force at the initial stages of the travel, which agrees with the analytical predictions. For $\theta_i > 45°$, the maximum of $f_{(es)}$ lies slightly above the 45° mark. Of all cases passing through $\theta = 45°$, the pair of discs starting from $\theta_i = 60°$ has the largest $f_{(es)}$ since the separation between discs is the smallest at $\theta = 45°$ (Fig. 3-b). The drop in force magnitude at smaller separation shows that the disc pair's orientation is the dominant factor.

4.2. The effect of Reynolds number

Reynolds number may be changed through various parameters (Eq. (4)). From a practical standpoint and for a given system, changing the electric field intensity is one of the most accessible

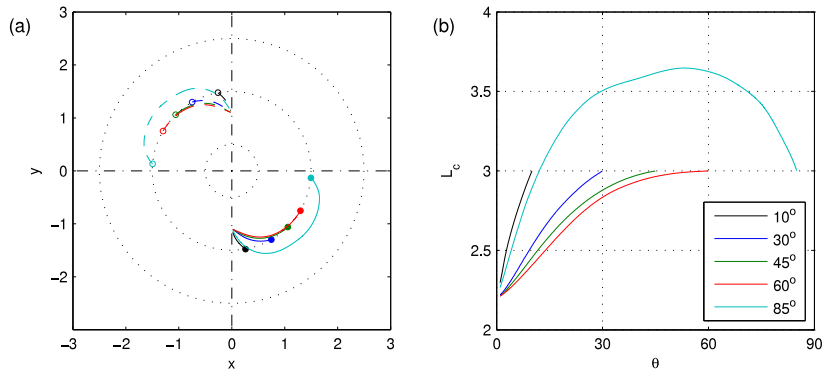

Fig. 3. (a) Trajectory of disc 1 (continuous) and disc 2 (dashed) with different starting angles; (b) center-to-center separation distance with respect to center-to-center angle with electric field. The middle dotted circle passes through the center of disc 1 for different cases while the inner and outer dotted circles are tangent to disc 1 in its initial position.

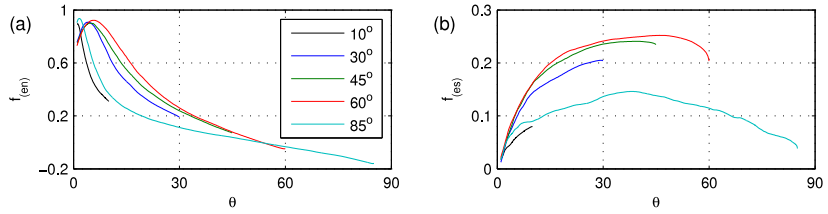

Fig. 4. Center-to-center (a) and rotational (b) components of electric forces with respect to angle.

control parameters. As a result, Reynolds number is manipulated through changes in the electric field here. Reynolds numbers calculated through Eq. (4) for particle chaining experiments in colloidal assembly process lie in $0.00001 < \mathrm{Re} < 0.01$ [2,11,12,36,37]. On the other hand, Reynolds numbers encountered in electrorheological flows are larger than those in colloidal assembly and may reach up to $\mathrm{Re} \approx 10$ [38–41]. Most numerical simulations in the literature only deal with very low-Reynolds regime of the chaining phenomenon [17–20]. Based on the observations made in the previous section, two initial angles of 45° and 85° are chosen for our tests. The electric field intensity is doubled in successive cases resulting in Reynolds numbers of 0.007, 0.028, 0.113, 0.453, 1.813, 7.253, 29.01 and 116.1.

Using Eq. (1) as well as balancing inertia and electric forces result in two characteristic time scales,

$$t_c = \frac{\mu_0}{\varepsilon_0 E_\infty^2}, \quad t_c' = \left(\frac{\rho_0 r_1^2}{\varepsilon_0 E_\infty^2}\right)^{\frac{1}{2}}, \tag{10}$$

respectively. Fig. 5 provides the chaining time with respect to Reynolds number in dimensionless form using both t_c and t_c'. The chaining time remains relatively constant with both starting angles for $\mathrm{Re} < 1$ when using t_c as the timescale. This confirms the observations made in [16] where the chaining time was found to be constant assuming a Stokes flow regime. The chaining time for $\mathrm{Re} > 1$ is relatively constant when t_c' is used for normalization. As a result, the chaining time in this study is proportional to E_∞^{-2} at lower Reynolds numbers and to E_∞^{-1} at higher Reynolds numbers.

Fig. 6 provides the trajectories and separation for starting orientations of 45° and 85°. In general, the discs follow a wider arc as Re increases. For $\mathrm{Re} \leq 0.113$, the trajectories hardly depend on Re. This is consistent with the small-Re results in [17]. As Reynolds number increases beyond 0.113, the disc trajectories become Re-dependent. For Reynolds numbers higher than unity, the discs may overshoot the $\theta = 0°$ line considerably, possibly making multiple passes across it. In such cases, the chaining is assumed to happen when the discs pass $\theta = \pm 1°$ with the electric field for the last time. At $\theta_i = 85°$ and $\mathrm{Re} = 116.1$, the initial separation becomes so large that the discs have negligible interaction and no chaining occurs. An overall comparison between $\theta_i = 45°$ and 85° shows that the effect of Re is much more pronounced at larger initial angle. The reason is the significant increase in separation at the initial stages for $\theta_i = 85°$ which reduces the magnitude of electrical forces (Fig. 6-b).

Table 2
Elapsed time for reaching θ_f at different $\mathcal{P}_r$ with $\theta_i = 45°$ and 85°.

$\mathcal{P}_r$	1	0.975	0.95	0.9	0.85	0.8	0.75	0.5	0.25
t_f ($\theta_i = 45°$)	10.76	11.05	11.21	11.33	11.48	11.61	11.90	13.03	16.71
t_f ($\theta_i = 85°$)	39.39	39.68	39.96	41.10	41.67	42.80	44.32	48.76	57.27

Similar to trajectories for $\mathrm{Re} \leq 0.113$, the electric forces are also insensitive to Re. The effects of increasing Re become more pronounced for $\mathrm{Re} \geq 0.453$ as the discs traverse wider arcs. However, the shift between repulsion and attraction in $f_{(en)}$ is independent of Re and happens at $\theta \approx 53°$.

4.3. The effect of difference in permittivity

Studies involving assembly of binary mixtures of colloidal particles such as yeast cells, NIH/3T3 mouse fibroblast cells, latex particles and iron oxide have been conducted experimentally [2,11,12]. However, to our knowledge, no previous study has investigated the interaction of dissimilar discs systematically, over a wide range of electrical permittivities. To simulate such conditions here, the permittivity of the first disc stays fixed at $\mathcal{P} = 40$, while that of the second disc decreases from $\mathcal{P} = 40$ to 10, resulting in disc-to-disc permittivity ratios of $\mathcal{P}_r = 1$, 0.975, 0.95, 0.9, 0.85, 0.8, 0.75, 0.5 and 0.25. Two initial orientations of 45° and 85° are considered and Re is set to 0.113. Chaining times for both starting angles, shown in Table 2, increase as $\mathcal{P}_r$ is reduced.

Fig. 7 plots the trajectories of the discs. These trajectories change little for $\mathcal{P}_r \geq 0.9$, especially for disc 1. The asymmetry in trajectory becomes more significant as $\mathcal{P}_r$ decreases, especially for $\mathcal{P}_r \leq 0.5$. In general, the chaining position of $\theta_i = 85°$ remains

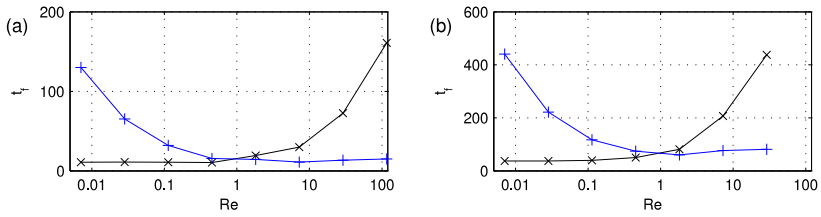

Fig. 5. Dimensionless time for reaching θ_f with respect to Reynolds number for starting angles of 45° (a) and 85° (b). The cross marks plot the chaining time normalized by t_c while plus marks show the chaining time normalized by t_c' (Eq. (10)).

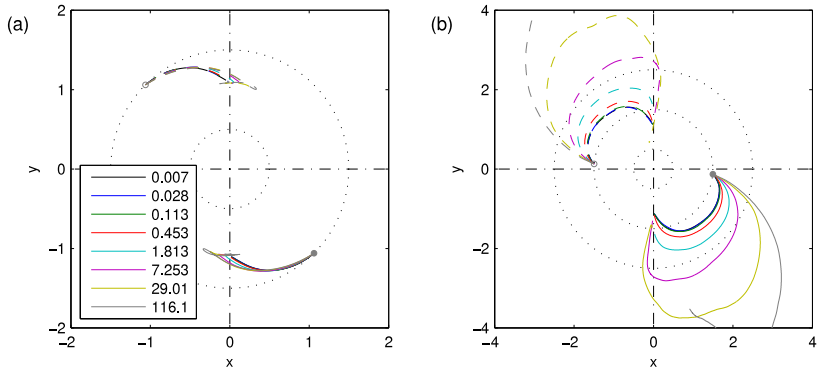

Fig. 6. Trajectory of disc 1 (continuous) and disc 2 (dashed) for $\theta_i = 45°$ (a) and 85° (b) at different Reynolds numbers.

close to the center of computational domain whereas for $\theta_i = 45°$ the chaining position skews toward upper-left quadrant. As $\mathcal{P}_r$ decreases, disc 1 follows a longer route while disc 2 traverses shorter arcs. The trajectories of dielectric discs presented here are quite different from those of conductive discs with zero permittivities. Kang [19] observes almost symmetric trajectories for the discs released from different initial orientations, regardless of up to 10 000 times difference in conductivities.

The reason behind the different routes taken by the discs is better explained in Fig. 8 where center-to-center and rotational components of the DEP forces are plotted for $\theta_i = 85°$. Since discs 1 and 2 experience different force magnitudes, both discs are shown in the figures. A general observation is that the force magnitudes are reduced at smaller $\mathcal{P}_r$, hence the larger chaining times observed in Table 2. Since electric forces are proportional to permittivity gradient (Eq. (9)), reducing the permittivity of disc 2 causes a dramatic reduction in DEP forces exerted on it. The smaller force magnitude on disc 2 explains the shorter path taken by the disc (Fig. 7). As the permittivity of disc 2 is reduced, its effect on the electric field lines becomes less pronounced. This results in an indirect reduction of DEP forces on disc 1 as the field lines around it become less asymmetric with decreasing $\mathcal{P}_r$.

The movement of the chaining location may be assessed based on the resultant force exerted on the disc pair taken as a single body at the midpoint of center-to-center line. As an example, we calculate the work done for $\mathcal{P}_r = 0.25$. The components for $\theta_i = 45°$ are 0.0921 and 0.3815 in x and y direction, respectively. The same components for $\theta_i = 85°$ are 0.0824 and 0.3155. While x-components are relatively close, the difference in y-components shows that the resultant forces in case $\theta_i = 45°$ is more inclined to carry the disc pair toward upper wall. When regarded as a single entity, the disc pair has a permittivity gradient pointing from disc 2 toward disc 1 which causes an electric force in the reverse direction. This explains the tendency of the disc pair to move toward the upper boundary.

4.4. Chaining of more than two discs

In general, DEP interactions happen among large numbers of interacting colloidal particles and biological cells, residing between co-planar electrodes [10–12] or parallel electrodes [36, 39,40]. To extend the observations made in previous sections, simulations with up to 36 discs are presented here. The domain size and fluid properties are kept similar to those of the previous sections.

Fig. 9 plots the chaining trajectory of three, four and five discs initially positioned in a circular arrangement where the distance between adjacent discs is $L_c = 3$. The angle θ_i between the line connecting the initial position of the reference disc (shown as two concentric circles) and the center of computational domain with the electric field is indicated above the plots. Reynolds number is set to Re = 0.113. Unlike the two-disc configuration of previous sections, the chain length here is comparable to the domain size. As a result, the chains are likely to move toward the top or bottom wall.

The top row of Fig. 9 shows the chaining process for identical discs with $\mathcal{P} = 40$. In general the discs form a single chain, however, two separate chains may be produced in certain orientations of four- and five-disc arrangements. For three discs in a triangular arrangement, each interacts strongly with its two neighbors, producing a single chain aligned with the field. If two of the discs are initially symmetric with respect to the y-axis, their order in the final chain is determined by numerical noise in the system. As the number of discs increases, the most significant interactions become limited to the closest neighbors. Here, the initial tendency to repel or attract a neighbor follows essentially the same rule as observed in Section 4.1. That is, assuming a disc and one of its neighbors as an adjacent pair, the region where center-to-center DEP force transitions from repulsion to attraction is about $\theta \approx 53°$.

Three orientations of four identical discs are shown in the top row of Fig. 9. In the y-axis symmetric arrangement at $\theta_i = 0°$, all adjacent pairs have a 45° angle with the electric field. This means $f_{(en)}$ is attractive for all adjacent pairs and the order of discs in the middle of the final chain is decided by numerical noise. On

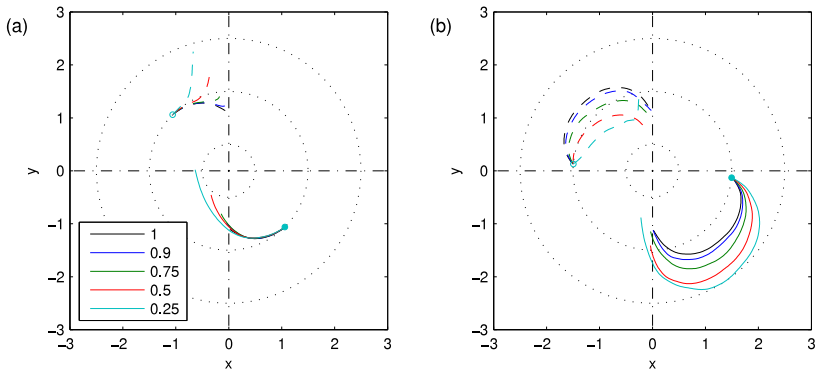

Fig. 7. Trajectory of disc 1 (continuous) and disc 2 (dashed) for $\theta_i = 45°$ (a) and 85° (b) with different disc-to-disc permittivity ratios.

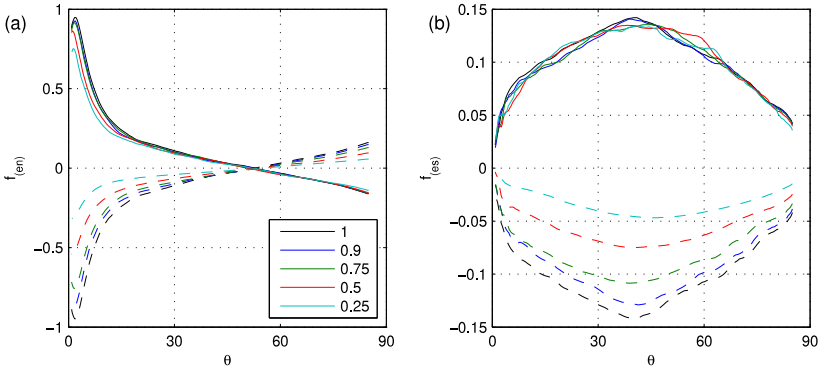

Fig. 8. Center-to-center (a) and rotational (b) components of DEP forces with respect to angle for $\theta_i = 85°$ for different disc-to-disc permittivity ratios. Solid lines are used for disc 1 while dashed lines are used for disc 2.

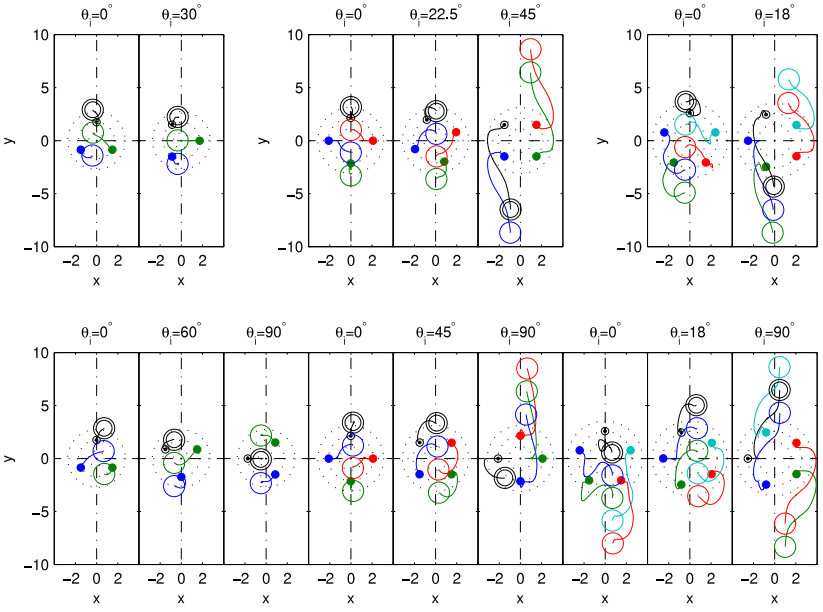

Fig. 9. Trajectories for three, four and five discs initially in a circular arrangement. Smaller filled circles denote the initial position of the discs. Larger circles show the final position of the discs and are drawn to scale. The reference disc is shown as two concentric circles. Initial orientation of the reference disc with the electric field is given above the respective plot. In the top row, all discs have identical properties. In the bottom row, the reference disc has half of the permittivity of the other discs.

the other hand, the order of discs is predictable at $\theta_i = 22.5°$. In this case, the reference disc and its neighbors initially form 22.5° and 67.5° angles with the electric field. As a result the reference disc forms a two-disc sub-chain with its left neighbor in the second quadrant while the remaining two discs form another sub-chain in the fourth quadrant. These sub-chains reside at an angle less than 90° with the field and as a result align with the electric field to form a single chain. For the y-axis symmetric arrangement at $\theta_i = 45°$, each disc repels one neighbor while attracting the other and the discs residing on each side of the y-axis form one sub-chain. Due to numerical noises, the line connecting the centers of these sub-chains deviates slightly from

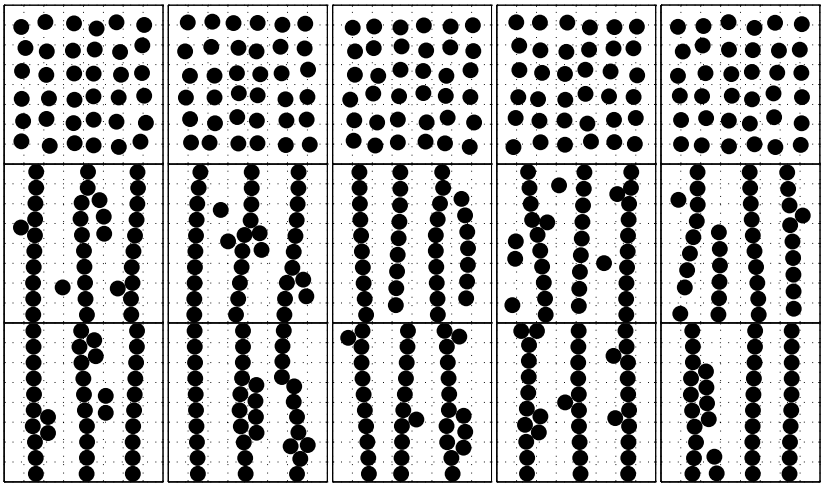

Fig. 10. Positions in chaining of 36 identical discs. Initial position of each column is shown at the top. Disc positions at $t = 25$ are shown for Re $= 0.113$ in the middle and for Re $= 116.1$ at the bottom. Time is scaled with t_c for Re $= 0.113$ while t_c' is used for Re $= 116.1$ (Eq. (10)).

90° with the electric field. While the sub-chains move to chain, the large angle with the electric field results in large separation and leads to divergence. The individual sub-chains travel toward opposite walls and remain separated. Similar observations are valid for five-disc arrangements.

To see the effects of having a particle with different electrical properties, the permittivity of the reference disc is halved for the bottom row of Fig. 9. The general preferences in regards to sub-chain formation of four- and five-disc arrangements remain valid here. Additionally, as mentioned in Section 4.3, the presence of a disc with lower permittivity skews the location of the sub-chain toward the initial position of the said disc. This breaks the y-axis symmetry of the centers of sub-chains and facilitates the formation of a single chain. As a result, halving the permittivity of the reference discs results in a single chain for four-particle arrangement at $\theta_i = 45°$ and five-particle arrangement at $\theta_i = 18°$. On the other hand, having a disc with lower permittivity results in different orientations with y-axis symmetric sub-chains, as seen in four- and five-particle arrangements at $\theta_i = 90°$.

To test the chaining of larger number of discs, we place them on a uniform Cartesian grid where adjacent discs are $L_c = 3$ apart. Then we apply a random perturbation of up to 0.4 in both x and y directions to the position of each disc to mimic likely experimental conditions. We observed the chaining behavior for 25 and 36 discs among 40 simulations. Fig. 10 shows five results from our simulations for 36 discs. The top row shows the initial configuration. The middle and bottom rows show chained configurations for Re $= 0.113$ and Re $= 116.1$, respectively, at $t = 25$. Time is scaled with t_c for Re $= 0.113$ while t_c' is used for Re $= 116.1$ (Eq. (10)). The maximum straight chain length is limited to 10 discs by the height of the computational domain ($H/r = 20$, Section 2). As a result, a minimum of two main chains for 25-disc case and three main chains for 36-disc case are formed. The remaining discs may form packed structures along the main chains, branch out from the main chains, create independent smaller chains or remain isolated during the simulation time. Applying periodic boundary conditions on the side walls of the computational domain had no significant effect on the overall arrangement of the discs observed here. The discs are more likely to create branches and smaller independent chains at low-Re. Qualitatively, the results look similar to the chains from the experiments presented in [11,12]. Unlike the non-chaining case for a pair of discs at Re $= 116.1$ and $\theta_i = 85°$ of Section 4.2, presence of adjacent discs recovers the chaining behavior. When compared to low-Re counterparts, branching is less likely to happen at larger Reynolds numbers. Instead, closely packed triangular structures are formed at parts of the main chains.

5. Conclusion

An incompressible smoothed particle hydrodynamics scheme is used to simulate the interaction of neutrally buoyant non-conductive circular discs suspended in quiescent medium subject to an external electric field. The trajectories of the discs for two reference cases of dielectrophoretic chaining are validated against literature data [17,18] to assess the accuracy of the method. The numerical method is then used to investigate the effects of changes in common variables in chaining, *i.e.* initial orientation, Reynolds number and unequal permittivity. Finally, the chaining behavior of multiple discs is briefly studied.

As there are no direct methods to measure the dielectrophoretic forces experimentally, there have been no comparisons of dielectrophoretic forces in prior numerical works [17,19,22]. To bridge this gap, we compare our crossover point of center-to-center dielectrophoretic force with analytical [1, 16] and experimental [14] data. Our results are in good agreement, showing that center-to-center and tangential components of forces derived from numerical methods are reliable analysis tools. We use this decomposition to study the interactions between multiple discs and predict their placement order.

While many studies deal with dielectrophoretic chaining in low Reynolds regime [17–20], high-Reynolds chaining is a less studied phenomenon. Here, we extend the Reynolds number regime to about 100, covering the range from assembly of colloidal particles to electrorheological flows. In agreement with [17], the trajectories show negligible difference at low Re. However, beyond Re ≈ 1 the trajectories become wider and possibly divergent. A more interesting effect of Re is on the chaining time which is proportional to E_∞^{-2} at lower Reynolds numbers and to E_∞^{-1} at higher Reynolds numbers. For multiple discs, the chains are likely to branch out in low Reynolds numbers, however, packed triangular structures are observed along the chains at larger Reynolds numbers.

Asymmetry of electrical properties is another common variable in dielectrophoretic interactions [2,11,12]. The effects of difference in conductivities are studied numerically in [19] in detail. To complement this, we investigated the effects of permittivity difference. Our results show that reducing permittivity of one disc results in longer chaining times and skews the chaining position toward the disc with lower permittivity. As a more practical application, we predict the position of the low-permittivity disc in a multi-disc chain by observing the cross-over angle and symmetry-breaking properties of the discs.

The current work elucidates the evolution of dielectrophoretic forces in terms of center-to-center and rotational components, increasing the confidence in numerical force data. As a next step, these observations have to be extended to more general particle shapes. Further studies may allow better prediction of chaining behavior based on system properties and achieving better control by changing field intensity.

Acknowledgments

NT, MO and MY gratefully acknowledge financial support provided by the Scientific and Technological Research Council of Turkey (TUBITAK) for [grant number 112M721]. NT additionally acknowledges financial support from Mitacs-Accelerate program, Canada under the [grant number IT08354]. AS gratefully acknowledges the financial support provided by the Natural Sciences and Engineering Research Council (NSERC), Canada for the Canada Research Chair in Computational and Experimental Mechanics. JJF was supported by NSERC, Canada, and acknowledges additional support by the Peter Wall Institute for Advanced Studies, Canada during his tenure as Wall Scholar, and the Isaac Newton Institute for Mathematical Sciences, United Kingdom for its hospitality supported by Engineering and Physical Sciences Research Council (EPSRC), United Kingdom [grant number EP/K032208/1]. Computational resources were supported in part by WestGrid, Canada (www.westgrid.ca) and Compute Canada Calcul Canada (www.computecanada.ca).

References

[1] M. Parthasarathy, D.J. Klingenberg, Electrorheology: Mechanisms and models, Mater. Sci. Eng. R-Rep. 17 (2) (1996) 57–103.
[2] O.D. Velev, S. Gangwal, D.N. Petsev, Particle-localized AC and DC manipulation and electrokinetics, Annu. Rep. Prog. Chem. C 105 (2009) 213–246.
[3] R. Pethig, Dielectrophoresis: Status of the theory, technology, and applications, Biomicrofluidics 4 (2) (2010) 022811.
[4] I.-F. Cheng, H.-C. Chang, D. Hou, H.-C. Chang, An integrated dielectrophoretic chip for continuous bioparticle filtering, focusing, sorting, trapping, and detecting, Biomicrofluidics 1 (2) (2007) 021503.
[5] N. Lewpiriyawong, C. Yang, Y.C. Lam, Dielectrophoretic manipulation of particles in a modified microfluidic h filter with multi-insulating blocks, Biomicrofluidics 2 (3) (2008) 034105.
[6] K.D. Hermanson, S.O. Lumsdon, J.P. Williams, E.W. Kaler, O.D. Velev, Dielectrophoretic assembly of electrically functional microwires from nanoparticle suspensions, Science 294 (5544) (2001) 1082–1086.
[7] X. Xiong, A. Busnaina, S. Selvarasah, S. Somu, M. Wei, J. Mead, C.-L. Chen, J. Aceros, P. Makaram, M.R. Dokmeci, Directed assembly of gold nanoparticle nanowires and networks for nanodevices, Appl. Phys. Lett. 91 (6) (2007) 063101.
[8] S.O. Lumsdon, E.W. Kaler, O.D. Velev, Two-dimensional crystallization of microspheres by a coplanar AC electric field, Langmuir 20 (6) (2004) 2108–2116.
[9] M. Yang, X. Zhang, Electrical assisted patterning of cardiac myocytes with controlled macroscopic anisotropy using a microfluidic dielectrophoresis chip, Sensors Actuators A 135 (1) (2007) 73–79.
[10] G.H. Markx, L. Carney, M. Littlefair, A. Sebastian, A.-M. Buckle, Recreating the hematon: Microfabrication of artificial haematopoietic stem cell microniches in vitro using dielectrophoresis, Biomed. Microdevices 11 (1) (2009) 143–150.
[11] S. Jain, S. Gupta, Dielectrophoretic coassembly of binary colloidalmixtures in AC electric fields, Langmuir 29 (52) (2013) 16105–16112.
[12] S. Gupta, R.G. Alargova, P.K. Kilpatrick, O.D. Velev, On-chip dielectrophoretic coassembly of live cells and particles into responsive biomaterials, Langmuir 26 (5) (2010) 3441–3452.
[13] T.B. Jones, Electromechanics of Particles, Cambridge University Press, 1995, http://dx.doi.org/10.1017/CBO9780511574498.
[14] H. Hwang, J.-J. Kim, J.-K. Park, Experimental investigation of electrostatic particle-particle interactions in optoelectronic tweezers, J. Phys. Chem. B 112 (32) (2008) 9903–9908.
[15] M. Mittal, P.P. Lele, E.W. Kaler, E.M. Furst, Polarization and interactions of colloidal particles in AC electric fields, J. Chem. Phys. 129 (6) (2008) 064513.
[16] K.H. Kang, D.Q. Li, Dielectric force and relative motion between two spherical particles in electrophoresis, Langmuir 22 (4) (2006) 1602–1608.
[17] Y. Ai, S. Qian, DC dielectrophoretic particle-particle interactions and their relative motions, J. Colloid Interface Sci. 346 (2) (2010) 448–454.
[18] C. Xie, B. Chen, C.-O. Ng, X. Zhou, J. Wu, Numerical study of interactive motion of dielectrophoretic particles, Eur. J. Mech. B-Fluids 49 (A) (2015) 208–216.
[19] S. Kang, Dielectrophoretic motion of two particles with diverse sets of the electric conductivity under a uniform electric field, Comput. Fluids 105 (2014) 231–243.
[20] M.R. Hossan, R. Dillon, A.K. Roy, P. Dutta, Modeling and simulation of dielectrophoretic particle-particle interactions and assembly, J. Colloid Interface Sci. 394 (2013) 619–629.
[21] D.L. House, H. Luo, S. Chang, Numerical study on dielectrophoretic chaining of two ellipsoidal particles, J. Colloid Interface Sci. 374 (2012) 141–149.
[22] Y. Ai, Z. Zeng, S. Qian, Direct numerical simulation of AC dielectrophoretic particle-particle interactive motions, J. Colloid Interface Sci. 417 (2014) 72–79.
[23] M.R. Hossan, R. Dillon, P. Dutta, Hybrid immersed interface-immersed boundary methods for AC dielectrophoresis, J. Comput. Phys. 270 (2014) 640–659.
[24] J.J. Monaghan, Smoothed particle hydrodynamics and its diverse applications, Annu. Rev. Fluid Mech. 44 (2012) 323–346.
[25] S.J. Cummins, M. Rudman, An SPH projection method, J. Comput. Phys. 152 (2) (1999) 584–607.
[26] A. Zainali, N. Tofighi, M.S. Shadloo, M. Yildiz, Numerical investigation of Newtonian and non-Newtonian multiphase flows using ISPH method, Comput. Methods Appl. Mech. Engrg. 254 (2013) 99–113.
[27] N. Tofighi, M. Yildiz, Numerical simulation of single droplet dynamics in three-phase flows using ISPH, Comput. Math. Appl. 66 (4) (2013) 525–536.
[28] N. Tofighi, M. Ozbulut, A. Rahmat, J.J. Feng, M. Yildiz, An incompressible smoothed particle hydrodynamics method for the motion of rigid bodies in fluids, J. Comput. Phys. 297 (2015) 207–220.
[29] M.S. Shadloo, A. Rahmat, M. Yildiz, A smoothed particle hydrodynamics study on the electrohydrodynamic deformation of a droplet suspended in a neutrally buoyant newtonian fluid, Comput. Mech. 52 (3) (2013) 693–707.
[30] D.A. Saville, Electrohydrodynamics: The Taylor-Melcher leaky dielectric model, Annu. Rev. Fluid Mech. 29 (1997) 27–64.
[31] IEEE-DEIS-EHD Tech Comm, Recommended international standard for dimensionless parameters used in electrohydrodynamics, IEEE Trans. Dielectr. Electr. Insul. 10 (1) (2003) 3–6.
[32] J. Hua, L.K. Lim, C.-H. Wang, Numerical simulation of deformation/motion of a drop suspended in viscous liquids under influence of steady electric fields, Phys. Fluids 20 (11) (2008) 113302.
[33] S. Vincent, J.C.B. de Motta, A. Sarthou, J.-L. Estivalezes, O. Simonin, E. Climent, A Lagrangian VOF tensorial penalty method for the DNS of resolved particle-laden flows, J. Comput. Phys. 256 (2014) 582–614.
[34] S. Koshizuka, A. Nobe, Y. Oka, Numerical analysis of breaking waves using the moving particle semi-implicit method, Internat. J. Numer. Methods Fluids 26 (7) (1998) 751–769.
[35] N. Tofighi, M. Ozbulut, J.J. Feng, M. Yildiz, The effect of normal electric field on the evolution of immiscible Rayleigh-Taylor instability, Theor. Comput. Fluid Dyn. 30 (5) (2016) 469–483.
[36] K.-Q. Zhang, X.Y. Liu, Controlled formation of colloidal structures by an alternating electric field and its mechanisms, J. Chem. Phys. 130 (18) (2009) 184901.
[37] J.J. Juarez, M.A. Bevan, Interactions and microstructures in electric field mediated colloidal assembly, J. Chem. Phys. 131 (13) (2009) 134704.
[38] N. Pannacci, E. Lemaire, L. Lobry, Rheology and structure of a suspension of particles subjected to quincke rotation, Rheol. Acta 46 (7) (2007) 899–904.
[39] E. Lemaire, L. Lobry, N. Pannacci, F. Peters, Viscosity of an electro-rheological suspension with internal rotations, J. Rheol. 52 (3) (2008) 769–783.
[40] H.-F. Huang, M. Zahn, E. Lemaire, Negative electrorheological responses of micro-polar fluids in the finite spin viscosity small spin velocity limit. i. Couette flow geometries, J. Electrostat. 69 (5) (2011) 442–455.
[41] Y.G. Ko, U.S. Choi, Negative electrorheological fluids, J. Rheol. 57 (6) (2013) 1655–1667.